INT. J. ELECTRONICS, 1998, VOL. 84, NO. 3, 187–202

Numerical simulation of an optoelectronic thyristor in the regime of incomplete turn-off

V. KOROBOV†, V. MITIN† and W. BUCHWALD‡

Direct two-dimensional simulations are used to analyse the possibility of controlling the carrier concentration in the gated base of a GaAs optoelectronic thyristor, which operates in the regime of incomplete turn-off. Modelling results indicate that the number of carriers, light intensity, current distribution, and the position of the light-emitting region the gated base of the thyristor can effectively be changed using gate currents, insufficient to turn the device completely off. The utilization of incomplete turn-off principle can be used for light-intensity modulation and switching purposes.

1. Introduction

Extensive research has been performed on III-V direct bandgap light-emitting thyristor-like PnpN structures (Simmons and Taylor l988, Crawford *et al.* 1988, Taylor and Cooke 1991, Kasahara *et al.* 1988, Buchwald *et al.* 1994, Heremans *et al.* 1994). Work by numerous researchers shows that these devices have many advantages over traditional pn light-emitting diodes and lasers due to their compatibility with key electrical elements of integrated circuits (Taylor and Cooke 1991), the capability of generating noticeable optical output for a small optical or electrical input (Simmons and Taylor 1988), and large-signal optical gain (Crawford *et al.* 1988). Optothyristors, based on III–V materials, are currently used as efficient light-triggerable devices (Taylor and Cooke 1991), laser drivers (Buchwald *et al.* 1994), elements of dynamic memories (Kasahara *et al.* 1988), optical amplifiers and optoelectronic switches (Heremans *et al.* 1992). Conventional applications of light-emitting thyristor-like structures as optoelectronic switches are based on the transitions between ON and OFF states. These transitions can be triggered by optical or electrical signals. It was suggested (Vagidov *et al.* 1995), that a third intermediate state of gate turn-off (GTO) thyristors may be interesting for an effective gate control of light-emitting thyristors. In this intermediate state (named the regime of the incomplete turn-off (Gribnikov *et al.* 1996) gate currents are not sufficient to turn the device off, and the middle pn junction is partially reverse biased and partially forward biased. For an appropriate value of the gate current J_g, this heterogeneous thyristor state is stationary and stable. The size of the central, highly conducting region depends on the applied gate current. Negative gate currents can squeeze the electron–hole plasma. If the anode current J_a is kept constant (i.e. if it is completely determined by the anode load resistance) we have the possibility of controlling the current density in the center of the device, the carrier concentrations, the local light-emitting intensity, and the total output power of radiation. The utilization of gate

Received 2 January 1997; accepted 2 June 1997.

† Department of Electrical and Computer Engineering, Wayne State University, Detroit, MI 48202, U.S.A.

‡ US Army Research Laboratory, Physical Sciences Directorate, Fort Monmouth, NJ 07703, U.S.A.

squeezing in light-emitting structures may provide new methods of controlling the optical output and essentially extend the functional capabilities of optothyristors by making direct modulation of the optical output independent of the carrier lifetime (Vagidov *et al.* 1995). The gated turn-off mechanism was first modelled by Wolley (Wolley 1966). His analytical description of turn-off was used as a guideline for design of GTO power thristors (Kurata *et al.* 1982, Azuma and Kurata 1988). Gribnikov and Rothwarf (1994) and Dutta and Rothwarf (1992) focused on the analytical calculation of storage and fall times when a negative voltage pulse, sufficient to switch the device completely off, is applied to the gate terminal. A steady-state theory for the potential distribution and current densities in the incomplete turn off regime has been developed (Vagidov *et al.* 1995, Gribnikov *et al.* 1996), which utilizes linear recombination mechanisms for the case of low base injection levels. This analytical approach assumes that the thyristor structure is infinitely long in the direction perpendicular to the current flow, and thus a quasi-one dimensional approximation holds. Analysis of the two-dimensional carrier distribution at high injection levels and arbitrary gate signals has not yet been carried out. Because an analytical approach has several natural limitations it is interesting to obtain an insight into the device operation in the incomplete turn-off mode using direct numerical modelling.

The goal of this paper is to present the results of exact two-dimensional simulations of a GTO thyristor, which operates in the regime of incomplete turn-off. Although significant work has been presented on thyristor-like optical switches, practically nothing exists on computer simulations of such devices, where an accurate physical model could play an important role in design and optimization. To date, most work has been done on the computer simulation of silicon power thyristors (Cornu and Lietz 1972, Herlet 1968, Kurata 1976, Adler 1978). Other research (Fardi 1994, 1996, Carson *et al.* 1989, 1991, Korobov and Mitin 1996) deals with the numerical simulation of III–V PnpN optical switches. The numerical approach developed by Fardi (1994, 1996) accounts for several important physical effects such as band-gap discontinuity, avalanche breakdown, and optical carrier generation. This approach also has current boundary conditions, which are more suitable for four-layer PnpN device, where terminal currents are single-valued in voltage for a given current under any circumstances. This model was successfully used for an analysis of steady-state current–voltage characteristics in III–V PnpN switches, and transient simulations were reported by Carson *et al.* (1991) and Korobov and Mitin (1996). Note that almost all the models cited above are one-dimensional, and the current squeezing effect is essentially a two-dimensional phenomenon. To evaluate the effects of applied gate voltage on steady-state and transient characteristics of gate-controlled optothyristors we have created a two-dimensional solver, which may be useful for the analysis and optimization of multi-terminal thyristor-like devices, operating in the regime of incomplete turn-off.

2. Numerical approach

The semiconductor device equations that we solve are Poisson's equation for electrostatic potential ψ

$$F_1(\xi) = \nabla \cdot \epsilon \nabla \psi - q(n - p + N_A - N_D) = 0 \qquad (1)$$

and time-dependent current continuity equations for electron and hole concentrations n and p:

$$F_2(\xi) = \frac{\partial n}{\partial t} - \nabla \cdot \frac{J_n}{q} + R(n,p) - G = 0 \tag{2}$$

$$F_3(\xi) = \frac{\partial p}{\partial t} + \nabla \cdot \frac{J_p}{q} + R(n,p) - G = 0 \tag{3}$$

Here J_n and J_p are electron and hole current densities, N_A and N_D are donor and acceptor concentrations, q is the electron charge and G is the rate of optical generation. ξ is a group of variables, consisting of n, p and ψ The recombination term in (2) and (3) accounts for three major mechanisms of generation–recombination: band-to-band radiative recombination R_{sp}, Hall–Shockley–Read R_{HSR} and Auger R_{Aug} terms:

$$R(n,p) = R_{sp} + R_{HSR} + R_{Aug} \tag{4}$$

$$R_{sp} = B_0(np - n_i^2) \tag{5}$$

$$R_{HSR} = \frac{np - n_i^2}{\tau_1(n + n_1) + \tau_2(p + p_1)} \tag{6}$$

$$R_{Aug} = (C_1 n + C_2 p)(np - n_i^2) \tag{7}$$

Material parameters correspond to GaAs. n_i stands for the intrinsic carrier concentration in GaAs, $B_0 = 7.7 \times 10^{-10}$ cm^3/s is the spontaneous recombination coefficient. The parameters of the HSR recombination are $\tau_n = \tau_p = 5 \times 10^{-7}$ s and $n_1 = p_1 = n_i$, the intrinsic concentration. R_{sp} gives the main contribution to the total recombination term $R(n, p)$ in (4). The impact ionization mechanism is not included in the current simulator because, as will be seen from our results, this effect is not important in the range of applied voltages under considerations. The temperature is assumed to be 300 K.

The box integration method (Selberherr 1984) has been used to discretize Poisson's equation. A Scharfetter–Gummel scheme (Scharfetter and Gummel 1969) has been implemented for the dicretization of the drift-diffusion continuity equations. A fully implicit finite difference scheme generates a nonlinear system of discrete equations

$$\boldsymbol{F}(\xi) = 0 \tag{8}$$

where $\boldsymbol{F}$ is a vector composed of the discretized forms of these three equations for all the grid points, and ξ is a vector form of n, p and ψ for the entire grid structure. This system of nonlinear equations has been solved by the Newton–Raphson method (Selberherr 1984). After linearization we obtain

$$\begin{pmatrix} \partial F_1/\partial\psi & \partial F_1/\partial n & \partial F_1/\partial p \\ \partial F_2/\partial\psi & \partial F_2/\partial n & \partial F_2/\partial p \\ \partial F_3/\partial\psi & \partial F_3/\partial n & \partial F_3/\partial p \end{pmatrix} \cdot \begin{pmatrix} \Delta\psi \\ \Delta n \\ \Delta p \end{pmatrix} = \begin{pmatrix} -F_1 \\ -F_2 \\ -F_3 \end{pmatrix}$$

or in short notations

$$\boldsymbol{F}'(\xi^{(m-1)})\,\Delta\xi^{(m)} = -\boldsymbol{F}(\xi^{(m-1)}) \tag{9}$$

where $\boldsymbol{F}'$ is the jacobian matrix of $\boldsymbol{F}$ and ξ^{m-1} is the vector form of the solution from the previous $(m-1)$th iteration and $\Delta\xi^m$ is the increment of ξ at the mth Newton iteration. The Yale Sparse Matrix Solver (Eisenstat *et al.* 1977) has been used for the inversion of the jacobian matrix at each iteration step.

3. Results and discussions

Figure 1 shows the geometry of the simulated PnpN gate turn-off thyristor (GTO). The simulated device is a rectangular structure where two outer emitter regions of 3 μm width (P and N) have doping concentrations 10^{17} cm^{-3}. The n- and p-bases are doped with 10^{15} cm^{-3} and have widths 10 μm and 4 μm, respectively. The sizes of the gate and cathode electrodes are 3 μm and 12 μm. The device length in the direction perpendicular to the current flow is 40 μm.

3.1. *ON state*

Generally, a thyristor exhibits a current-controlled type of switching characteristic. The static thyristor voltage is uniquely defined as a single-valued function of the current, which is not the case if the thyristor current is viewed as a function of the voltage. In general, there are three currents that correspond to a given voltage: one in

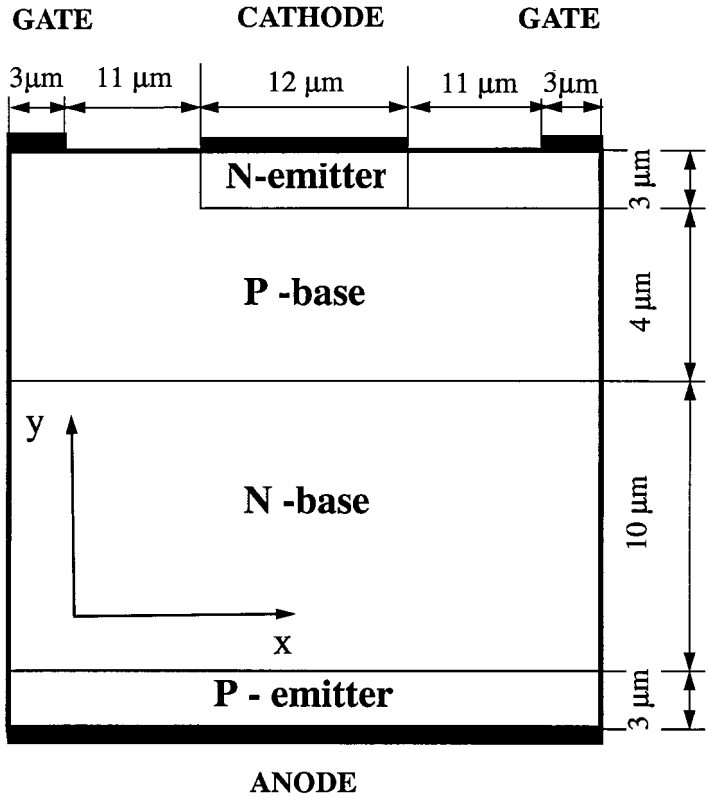

Figure 1. The geometry of the simulated thyristor.

the forward blocking branch, the second in the holding branch, and the third in the conduction branch. Thus, in a purely theoretical sense, it is unknown which of the operating conditions is reached as a consequence of the numerical convergence. In the regime with fixed electrode current the current–voltage characteristic is a single-valued function of the current. The inclusion of current boundary conditions requires the integration of current density along a contact. Discretizing this form of boundary condition introduces far neighbour interactions which destroy the pentadiagonal nature of the jacobian and often complicates the solution of the set of linear equations due to the convergency problems (Adler *et al.* 1987). In practice, this fact imposes strict limitations on the magnitudes of current increments, if the solution at the previous bias is used as an initial guess for the next bias. It has been shown (Kurata 1976) that if the initial trial conditions are close to the true solution for the ON state, this solution can be obtained using the voltage-controlled type of boundary conditions. A similar argument holds for the forward blocking state. In a one-dimensional problem, Kurata (1976) used an analogy between thyristors in the fired state and p-i-n rectifiers to reach an upper branch of the I–V characteristics.

In the two-dimensional problem to reach the ON state solution we proceed as follows. After obtaining the solution for the zero bias, we then decrease the cathode voltage at a fixed anode and gate potential. The anode is assumed to be grounded, and the gate potential is kept equal to its built-in potential. The decrease of the cathode voltage means that the gate effectively becomes positive with respect to cathode and thus positive gate current increases the carrier concentrations in the p-base. The excess carriers provide the biasing action which cause a decrease of potential barrier of the middle junction and the thyristor turns on. Next, we fix the cathode potential and total anode current. Now currents through the gate electrodes can be changed and we can study the effects of gate current on carrier and potential distributions. This procedure was found to be useful for the reduction of the total computational time. Figure 2(*a*) shows the carrier distributions along the centre of the device for the anode current $I_a = 0.28\,\mathrm{A/cm}$ and no gate currents. The electron $n(x,y)$ and hole $p(x,y)$ concentrations are found to be nearly uniform and almost equal to each other in both bases (i.e. $n(x,y) \simeq p(x,y) \simeq 3 \times 10^{16}\,\mathrm{cm}^{-3}$ at $3\,\mu\mathrm{m} < y < 17\,\mu\mathrm{m}$), and much greater than the background doping concentrations ($10^{15}\,\mathrm{cm}^{-3}$). From Fig. 2(*b*) one can see that potential barrier across the middle pn junction practically disappears due to high injection level in both bases.

3.2. *Gate squeezing effects*

The application of a negative gate bias causes the removal of excess holes through the gate contact. The removal of holes is accompanied by a removal of electrons to maintain space charge neutrality. Because the removal of one type of carrier is always balanced by the removal of a carrier of the opposite type, following Wolley (1966) we concern ourselves with only one type of excess carrier, which in this case we choose to be electrons. Fig. 3 shows the electron concentration for the gate current $I_g = 0.028\,\mathrm{A/cm}$ which corresponds to a gate potential of $-4.2\,\mathrm{V}$. It is seen that in the regions adjacent to the gates the electron concentration decreases drastically. Analysis of the hole distribution shows a concentration that is equal to the equilibrium value of $p = 10^{15}\,\mathrm{cm}^{-3}$ in these regions. The number of holes starts decreasing in the n-side of the middle pn junction at $y = 13\,\mu\mathrm{m}$. It is clear from Fig. 2 that in the p-base excess holes and electrons are present only in the central

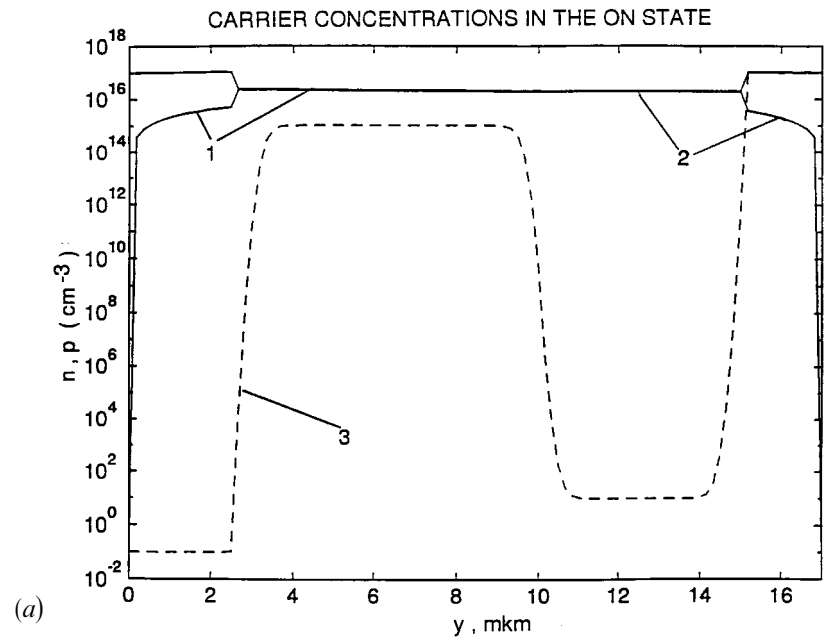

(*a*)

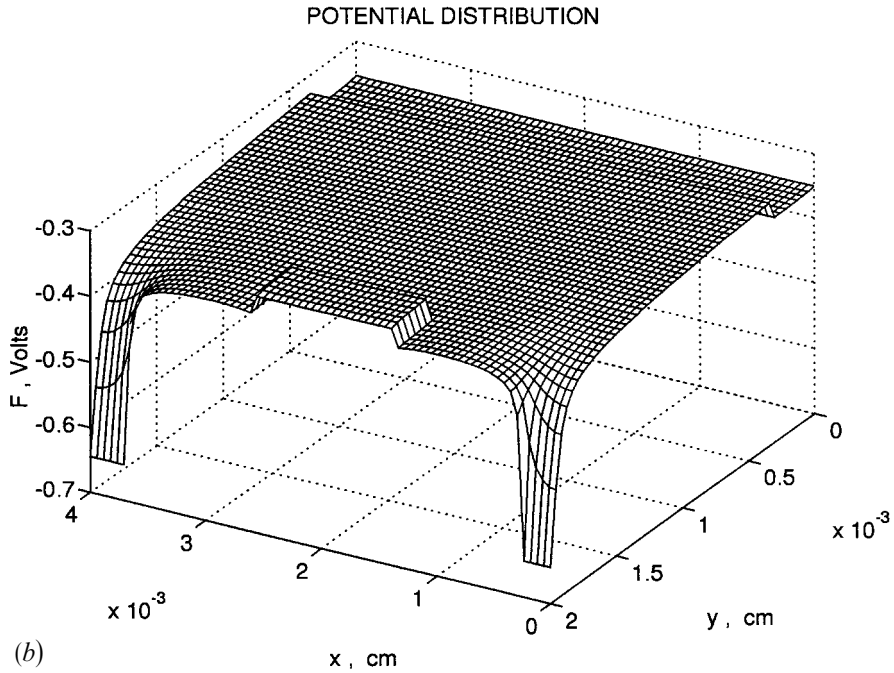

(*b*)

Figure 2. (*a*) Electron and hole concentrations in the ON state along the centre of the device with anode current $I_a = 0.28\,A/cm$ and no gate currents; in the inner regions at $3\,\mu m < y < 17\,\mu m$ carrier concentrations are very close to each other ($n \simeq p \simeq 3 \times 10^{16}\,cm^{-3}$); curves 1 and 2 correspond to electron and hole densities. The dashed line 3 shows equilibrium electron distribution. (*b*) Electrostatic potential distribution for the same anode current; there is no potential barrier across the middle pn junction.

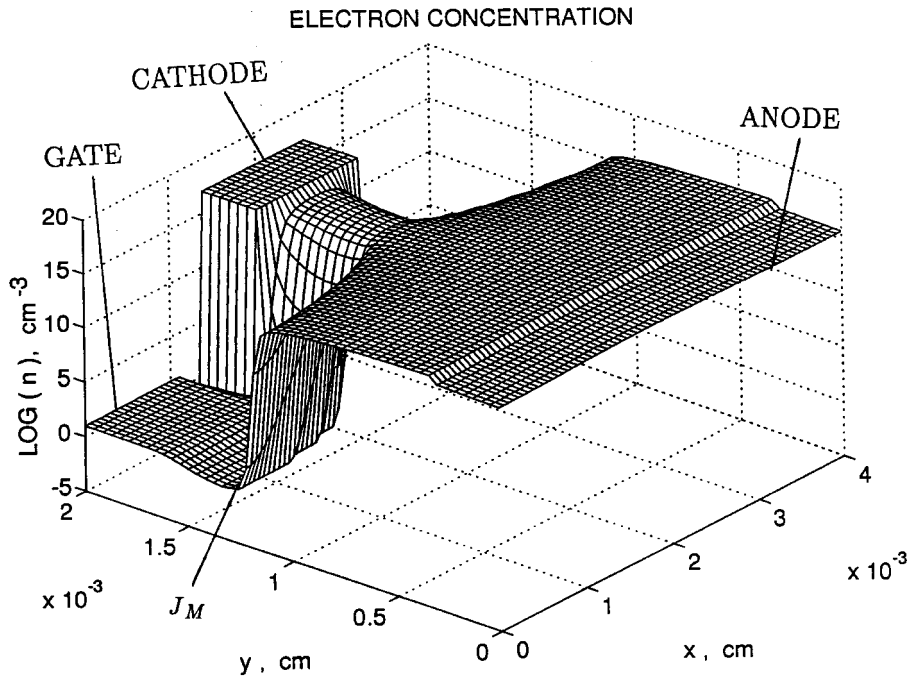

Figure 3. Electron concentration plot in the regime of optothyristor incomplete turn-off; distribution corresponds to the anode current I_a = 0.28 A/cm and two equal gate currents $J_{g1} = J_{g2}$ = 0.028 A/cm; J_M indicates the location of the middle pn junction.

part of the device. Due to carrier removal, portions of the middle pn-junction J_M come from saturation, and depletion regions with high electric fields (see Fig. 4) are formed near the gates. As can be seen in Fig. 5 these regions are low-conducting, and they block the current.

The driven decrease of carrier concentrations in the p-base makes the cathode-p-base junction also partially reverse biased. Fig. 5 shows that the current density at the cathode-p-base junction is squeezed and electrons are injected only from the central part of the cathode. From Fig. 3 it is clearly seen that there is a heterogeneous state of carrier distribution inside the thyristor with two substantially different regions of high and low concentrations. The transition layer between regions is relatively thin, thus the carrier squeezing effect is well pronounced. From the above it is obvious, that light emission due to spontaneous recombination in the p-base would be concentrated in the centre of the device and would be negligible in the depletion regions. Fig. 6 shows the distribution of the spontaneous recombination rate, calculated using (5), in the controlling p-base. There is a sharp maximum at the centre of the device, where excess carriers are present. The number of emitted photons from the central part of the device is many orders of magnitude greater than the radiation from the unsqueezed region. This well pronounced squeezing effect gives us a hope that an experiment to demonstrate the proof of principle behind PnpN structures operating in an incomplete turn off mode can be successful. Light from the unsqueezed portion of the devices probably will not substantially limit the ability to detect the modulated optical signal due to the applied gate currents.

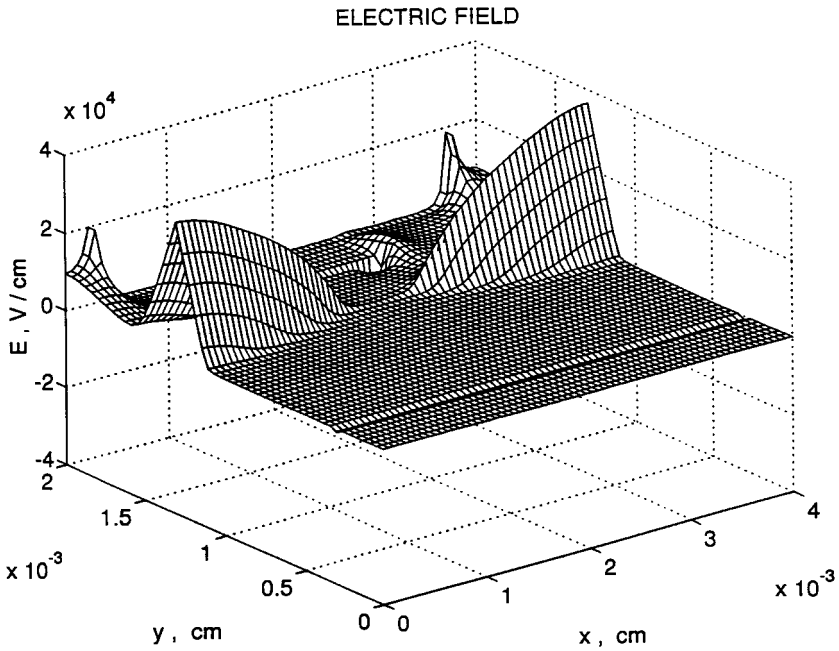

Figure 4. Electric field distribution for the same currents as in Fig. 3; areas of high electric field correspond to the reverse biased middle p-n junction; the central part of the junction is still forward-biased.

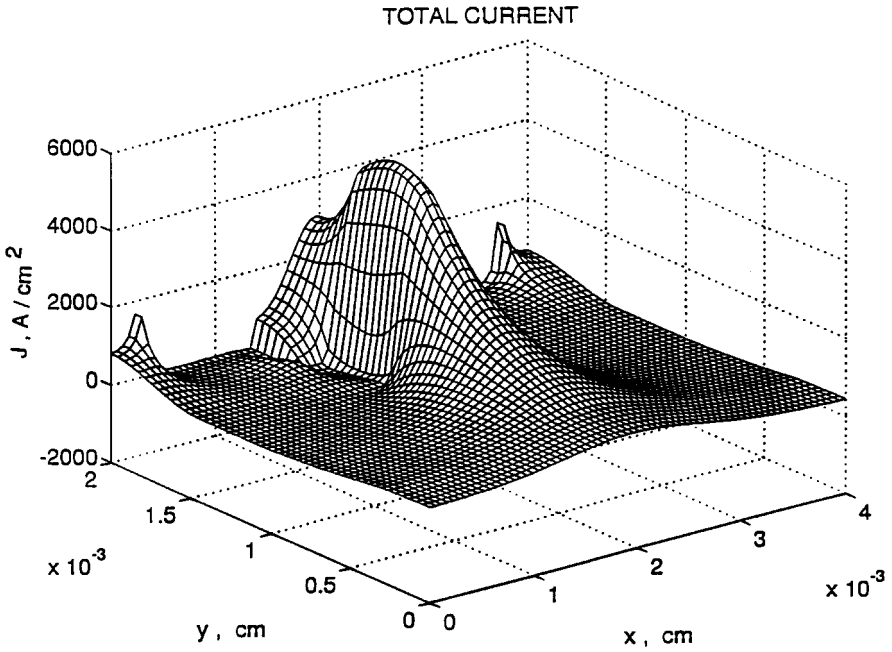

Figure 5. Lateral component of current density J in the thyristor incomplete turn off regime; total gate and anode currents are the same as in Fig. 3; the current is squeezed towards the centre of the device and flows in the regions, where the middle and cathode-p-base junctions are forward-biased.

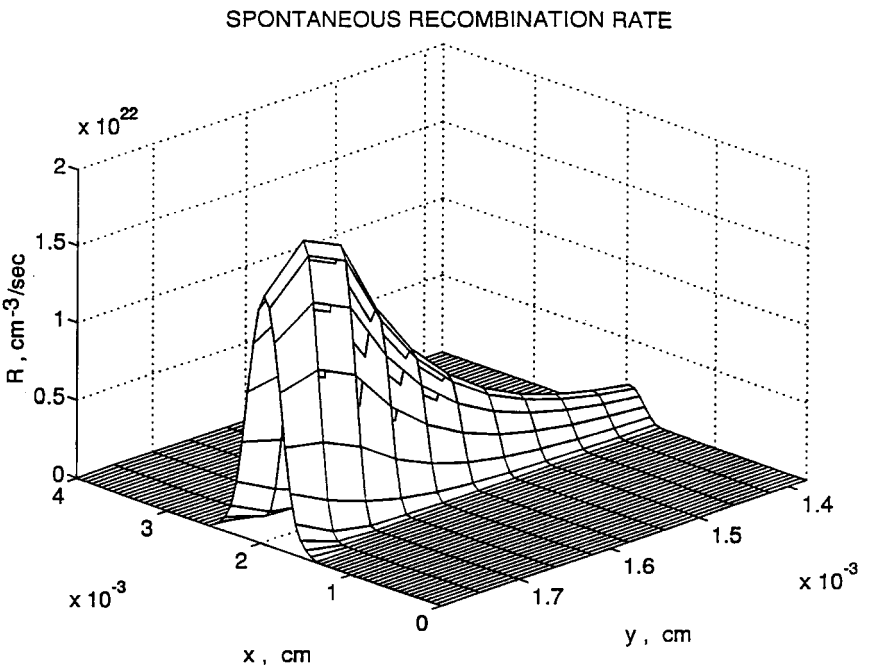

Figure 6. Rate of spontaneous recombination in the controlling p-base for the same anode and gate currents as in Fig. 3.

The distributions in Figs 3–6 were plotted for the ratio of currents $I_a/J_g = 10$. Thus the gate current, which is only 10% of the anode current, causes this dramatic inhomogeneous carrier distribution.

Our analysis has shown that a well-pronounced squeezing effect depends on the magnitude of the anode current and geometrical device parameters. If the anode current is too small, the device will be turned off before the central conducting channel is formed. For the simulated structure it was impossible to obtain essentially inhomogeneous carrier distributions if the anode current was less than 0.05 A/cm. At these anode currents a gate voltage changed the carrier distribution, but regions with small and large concentrations separated by a narrow boundary did not appear. Instead, the voltage drop across the device increased sharply and the device was turned completely off. At high anode currents there is another limitation to the applied gate signal. At a high negative gate bias the regions of high electric field at the edges of the middle pn-junction become wide enough to reach the gate electrode. In this case the size of the conducting channel in the p-base cannot be controlled. Making the p-base wider is not desirable, because then higher gate currents are required to squeeze the electron–hole plasma. However, a higher doping of the p-base would solve this problem. It was also found that the width of the n-base is very important in controlling the size of the conducting region with a small gate signal. In the structure presented here, the hole current is concentrated in the centre of the device. If some fraction of the injected holes reaches the region of the reverse biased middle pn junction they will be carried to the gates by the strong electric field of the depletion region. These holes contribute to the parasitic gate current flowing through the Pnp transistor. This current is not related to the squeezing of

the conducting region and decreases the sensitivity with respect to the gate control. It was found that if we decreased the width of the n-base by a factor of two and kept the same initial excess carrier concentrations, then the gate current required to achieve the same size of the conducting channel as in Figs 3–6, was even higher than the device total anode current.

For the structure presented here an increase of current density in the centre of the device was accompanied by an increase in the anode–cathode voltage drop. The carrier concentration in the conducting region was found to monotonically decrease with an increase of the negative gate voltage. An increase in the carrier concentration by up to 10% due to the current squeezing, in comparison with the zero gate signal case, was found in the wider structure with a device cross-section of $100 \times 200\,\mu$m. For this wider structure during the initial stage of gate turn-off the carrier concentration was found to increase slightly in the centre of the device and then decrease in a fashion, similar to the narrower device.

At gate currents greater than 0.03 A/cm the supply of holes into the plasma region is no longer sufficient to sustain a flow of electrons across the p-base. For $J_g > 0.035$ A/cm the anode voltage drop increases rapidly and a potential barrier develops across the whole area of the middle p-n junction. This means that the critical gate current J_g^{cr}, which determines the upper boundary of the incomplete turn-off regime (Wolley 1966) for the simulated structure, is approximately $J_g^{cr} = 0.035$ A/cm. The electric field distribution for $J_g = 0.04$ A/cm is plotted in Fig. 7. Regions of high electric field reached each other and the whole middle pn junction is reverse-biased. The carrier concentration at a given gate current

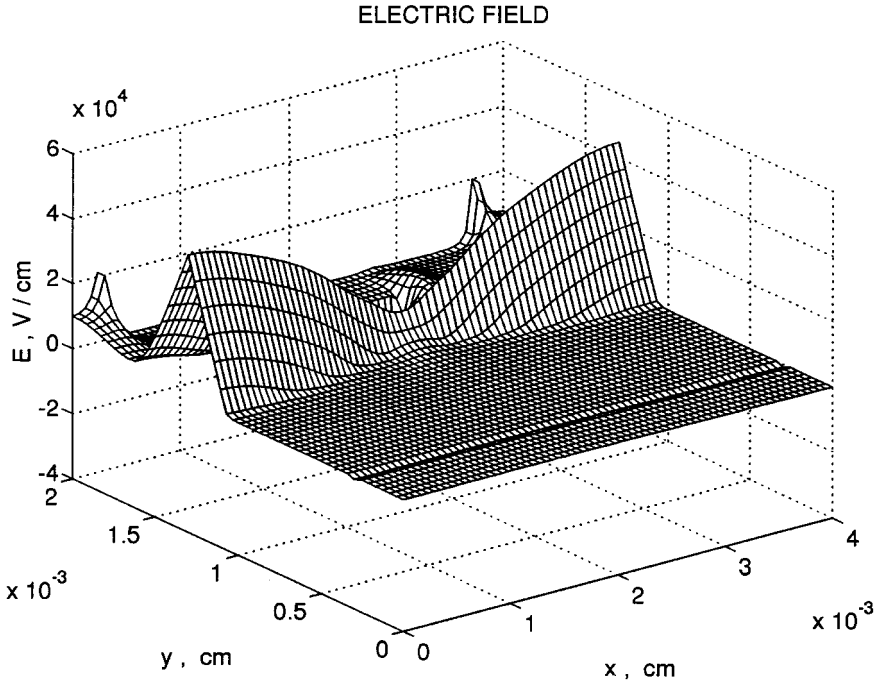

Figure 7. Electric field distribution for anode current $I_a = 0.28$ A/cm and gate currents $J_g = 0.04$ A/cm; the whole middle pn junction is reverse-biased.

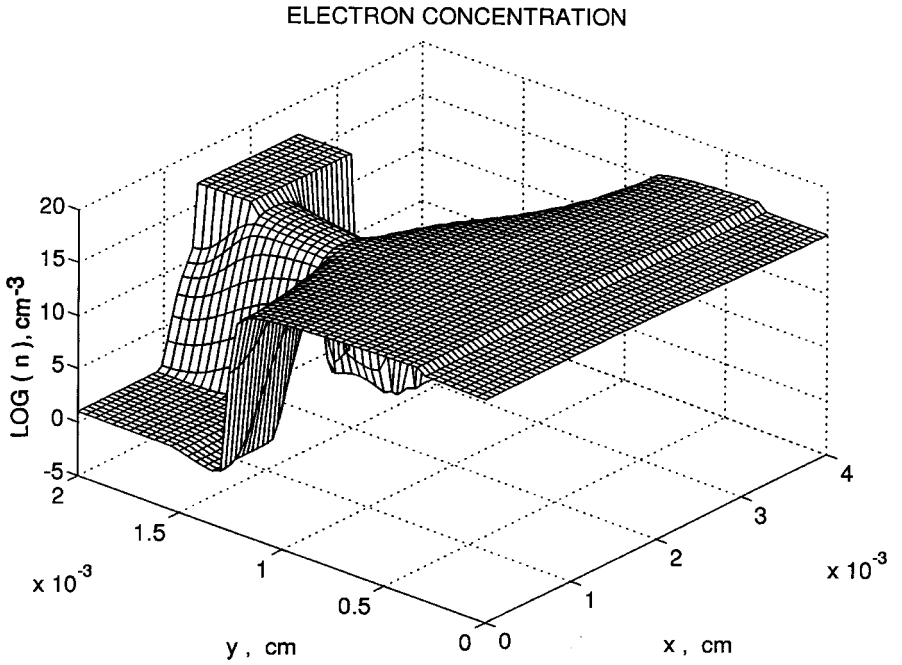

(*a*)

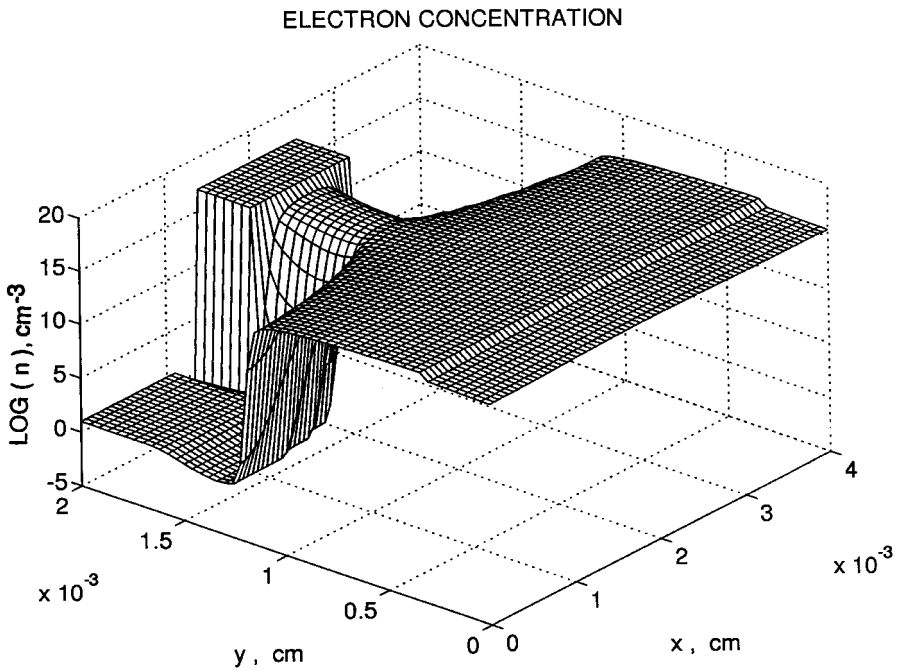

(*b*)

Figure 8. Shift of electron density distribution due to the different gate currents: (*a*) ratio of currents $J_{g2}/J_{g1} = 2.63$; (*b*) Gate current ratio is $J_{g1}/J_{g2} = 2.63$.

decreases, almost up to the equilibrium values. Thus, the conducting regions shrinks to a very narrow filament and the device turns off.

3.3. *Shift of the conducting channel*

We have considered the case where equal currents, flowing through each gate, control the size of the conduction region. Dual gates make it possible to control the position of the light-emitting region. This control can be used for a new type of optical space division switches. The major component of the switches is a device that can direct light in one of several directions in reaction to an external control (Lu *et al.* 1995, Yao and O'Mahony 1994, Kalman *et al.* 1992).

To study the possibility of the conducting channel shift we have simulated the GTO thyristor with different gate currents J_{g1} and J_{g2}, flowing through the left and right gates. Results are presented for the ratios $J_{g1}/J_{g2} = 0.38$ and $J_{g1}/J_{g2} = 2.63$. The total gate current $J_g = J_{g1} + J_{g2}$ was constant for both cases and was equal to $J_g = 0.05$ A/cm. Figs 8(*a*) and 8(*b*) indicate that for these gate current ratios the conducting region can be shifted to one or the other edge of the cathode without changes in the width of the conducting channel. It is seen that the region of high carrier concentrations is located closer to the gate with the smaller current. The shift of the blocking regions causes a shift in the position of the maximum total current density and of the maximum of carrier concentrations. The spontaneous recombination rate, given by (5), is shown in Fig. 9 for the gated base. Two maxima correspond to the same gate currents ratios as in Fig. 8. From the distribution of the spontaneous recombination rate, shown in Fig. 9, it is possible to conclude that the shift of

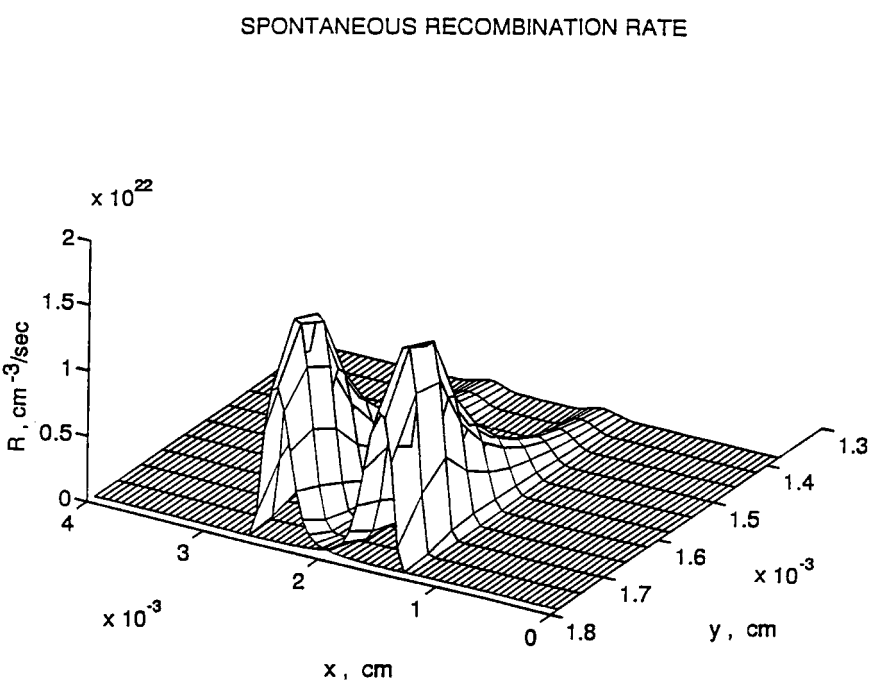

Figure 9. Two plots of spontaneous recombination rate, calculated for carrier distributions shown in Figs 8(*a*) and (*b*).

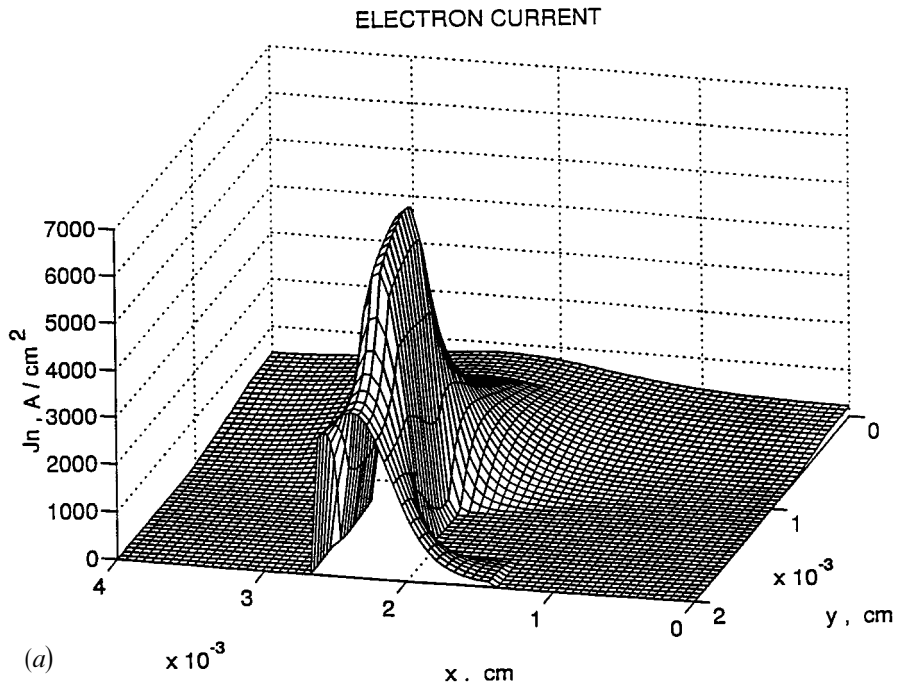

(*a*)

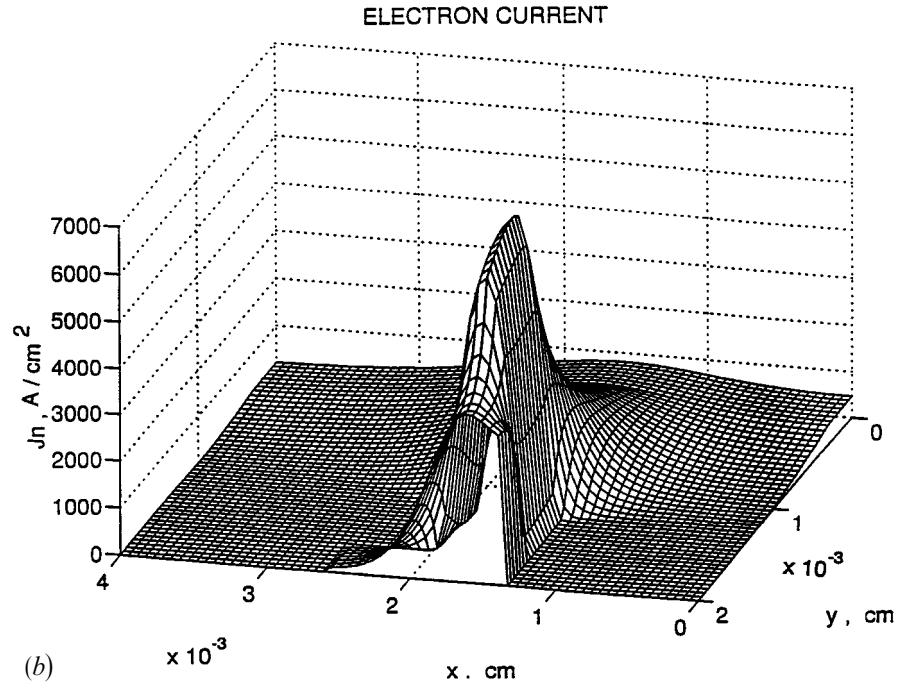

(*b*)

Figure 10. Results of transient simulation when the gate current ratio J_{g1}/J_{g2} was changed from 2.63 to 0.38: (*a*) electron current distribution at $t = 0$; (*b*) electron current density at $t = 0.5$ ns.

light intensity across the p-base is greater than a half-width of the channel region when gate currents were equal to zero, and is approximately equal to the whole length of the cathode (12 μm).

We have also performed transient simulations, where gate current ramps were applied to the gates. The initial carrier distribution corresponds to Fig. 8(*a*). At $t = 0$ the gate currents have been changed so that their ratio became 2.63. Simulation results show that it takes approximately 0.5 ns for the electron distribution to coincide with the plot of Fig. 8(*b*). The distribution of the electron current density at $t = 0.5$ ns is shown in Fig. 10(*b*). Although the transient process did not finish at this time, carrier concentrations demonstrate a well-defined maximum, very similar to that in Fig. 8(*b*), at the right edge of the anode. Thus, the shift of the conducting region over a distances nearly 12 μm occurs during 0.5 ns. It is easy to estimate that channel shifts over distances, comparable with the GaAs radiation wavelength may be made during time intervals of order 0.1 ns. This fact may lead to a new design of fast optoelectronic devices, where optical switching could be based on the shift of the light-emitting region.

4. Conclusion

We have performed exact two-dimensional simulations of a GaAs GTO light-emitting thyristor, which operates in the regime of incomplete turn-off. Simulation results show that relatively small gate currents can create inhomogeneous current and carrier distributions, and thus make possible effective gate control of light emission in optoelectronic thyristors. The size of the conducting region was found to be a sensitive function of applied gate current, which squeezes the electron–hole plasma towards the centre of the device. Small gate currents change the rate of spontaneous recombination by many orders of magnitude in a large area of the device. This can be used for light-intensity modulation in light-emitting devices, as well as in optical switching applications. The device can be further optimized by the addition of heterojunctions for the confinement of light or a Fabry–Perot cavity for lazing.

We have demonstrated numerically the possibility of shifting the current-conducting region in the case of asymmetric gate currents. In our simulation this shift was found to be at least 12 μm, which is larger than the width of the conducting light-emitting region. Shifts of the emitting region can be used to create a new type of logic optothyristors or memory cell. Simulation results show that switching times in the subnanosecond range can be obtained in this type of device.

Acknowledgment

This work was supported by the NSF.

References

Adler, M. S., 1978, Accurate calculations of the forward drop and power dissipation in thyristors. *IEEE Transactions on Electron Devices*, **25**, 16–22.

Adler, M. S., Pattnayak, D. N., Baliga, B. J., Temple, V. K., and Chang, H. R., 1987, Device physics and modelling of integrated power devices. *Proceedings of the Fifth International Conference on the Numerical Analysis of Semiconductor Devices and Integrated-Circuits*, pp. 1–19.

AZUMA, M., and KURATA, M., 1988, GTO thyristors. *Proceedings of the IEEE*, **76**, 419–427.

BUCHWALD, W. R., ZHAO, J. H., ZHU, L., SCHAUER, S., and JONES, K. A., 1994, A three terminal InP/InGaAsP optoelectronic thyristor. *IEEE Transactions on Electron Devices*, **41**, 620–622.

CARSON, R. F., HUGHES, R. C., ZIPPERIAN, T. E., WEAVER, H. T., BRENNAN, T. M., HAMMONS, B. E., and KLEM, J. F., 1989, Radiation responce of optically-triggered GaAs thyristors. *IEEE Transactions on Nuclear Science*, **36**, 2147–2154.

CARSON, R. F., HUGHES, R. C., and WEAVER, H. T., 1991, Long switching delay mechanisms for optically triggered GaAs thyristors. *Applied Physics Letters*, **59**, 834–836.

CORNU, J. and LIETZ, M., 1972, Numerical investigation of the thyristor forward characteristic. *IEEE Transactions on Electron Devices*, **19**, 975–981.

CRAWFORD, W., TAYLOR, G., COOKE, P., CHANG, T. Y., TELL, B., and SIMMONS, J., 1988, Optoelectronic transient response of the self-aligned double heterostructure optoelectronic switch. *Applied Physics Letters*, **53**, 1797–1799.

DUTTA, R., and ROTHWARF, A., 1992, A new analytical model for gated turn-off of thyristors. *IEEE Transactions on Electron Devices*, **39**, 1752–1757.

EISENSTAT, S. C., GURSKY, M. C., SCHULTZ, M. H., and SCHERMAN, A. N., 1977, The Yale sparse matrix package 2: The nonsymmetric codes. Technical report 114, Yale University.

FARDI, H. Z., 1994, Simulation and modelling of p-n-p-n optical switches. *IEEE Transactions on Computer-Aided Design of Integrated Circuits and Systems*, **12**, 666–671; 1996, Effects of interface and bulk recombination on switching characteristics of AlGaAs/GaAs pnpn bistable device. *IEEE Transactions on Electron Devices*, **42**, 2248–2250.

GRIBNIKOV, Z, and ROTHWARF, A., 1994, A new intermediate state model for the GTO: relation to the turn-off process. *Solid-state Electronics*, **37**, 135–139.

GRIBNIKOV, Z. S., KORSHAK, A. N., VAGIDOV, N. Z., and MITIN, V. V., 1996, Effect of base parameters on gate-controlled squeeze of current-conducting region in pnpn structures. *Solid-state Electronics*, **39**, 915–922.

HEREMANS, P. L., KUIJK, M., and BORGHS, G., 1992. Fast turn-off of two-terminal double-heterojunction optical thyristor. *Applied Physics Letters*, **61**, 1326–1328.

HEREMANS, P., KUIJK, M., VOUNCKX, R., and BORGHS, G., 1994, Properties and applications of optical thyristors, *Journal de Physique*, **4**, 2391–2404.

HERLET, A., 1968, The forward characteristics of silicon power rectifiers at high current densities. *Solid-state Electronics*, **11**, 717-742.

KALMAN, R. F., KAZOVSKY, L. G., and GOODMAN, J. W., 1992, Space division switches based on semiconductor optical amplifiers. *IEEE Photonics Technology Letters*, **4**, 1048-1049.

KASAHARA, K., TASHIRO, Y., NAMAO, N., SUGIMOTO, M., and YANASE, T., 1988, Double heterostructure optoelectronic switch as a dynamic memory with low-power consumption. *Applied Physics Letters*, **52**, 679–681.

KOROBOV, V., and MITIN, V., 1996, Reverse recovery of a GaAs optoelectronic thyristor. *Journal of Applied Physics*, **79**, 1143-1150.

KURATA, M., 1976, One-dimensional calculation of thyristor forward voltages and holding currents. *Solid-state Electronics*, **16**, 681–688.

KURATA, M., AZUMA, M., OHASHI, H., TAKIGAMI, K., NAKAGAWA, A., and KISHI, K., 1982, Gate turn-off thyristors. *Semiconductor Devices for Power Conditioning* (New York; Plenum), pp. 91–119.

LU, Y-C., CHENG, J., ZOLPER, J. C., and KLEM, J., 1995, Integrated optical/optoelectronic switch for parallel optical interconnects. *Electronics Letters*, **31**, 579–580.

SCHARFETTER, D. L., and GUMMEL, H. K., 1969, Large-signal analysis of a silicon Read diode oscillator. *IEEE Transactions on Electron Devices*, **16**, 64–77.

SELBERHERR, S., 1984, *Analysis and Simululation of Semiconductor Devices* (New York: Springer-Verlag).

SIMMONS, J., and TAYLOR, G., 1988, Electronic conduction and generation mechanism in the double heterostructure optoelectronic switch (DOES). *IEEE Trancsactions on Electron Devices*, **35**, 1278–1284.

TAYLOR, G., and COOKE, P., 1991, Determination of the switching condition in the quantum-well double-heterostructure optoelectronic switch (DOES). *IEEE Transactions on Electron Devices*, **39**, 2529–2541.

VAGIDOV, N. Z., GRIBNIKOV, Z. S., KORSHAK, A. N., and MITIN, V. V., 1995, Intermediate state of a controllable four-layer p-n-p-n structure. *Semiconductors*, **29**, 1021-1029.

WOLLEY, E., 1966, Turn-off in pnpn devices. *IEEE Transactions on Electron Devices*, **13**, 590–597.

YAO, J., and O'MAHONY, M. J., 1994, Experimental study of semiconductor laser amplifiers for photonic time and space switching amplifiers. *International Journal of Optoelectronics*, **9**, 219–220.